Hybrid Advances 13 (2026) 100639

Contents lists available at ScienceDirect

Hybrid Advances

journal homepage: www.journals.elsevier.com/hybrid-advances

Research Article

Green inhibition of microbiologically influenced corrosion on 316L stainless steel by *Artemisia annua* extract

Gloria Zlatić Jelić [a,*], Ivana Martinović [a], Zora Pilić [a], Janez Kovač [b], Marcela Romić [c]

[a] Department of Chemistry, Faculty of Science and Education, University of Mostar, Matice Hrvatske bb, Mostar, 88 000, Bosnia and Herzegovina
[b] Jozef Stefan Institute, Department of Surface Engineering, Jamova 39, Ljubljana, 1000, Slovenia
[c] Department of Physical Medicine and Rehabilitation, Clinical Hospital "Sveti Duh", Zagreb, 10 000, Croatia

ARTICLE INFO

Keywords:
Pseudomonas aeruginosa
Biofilm formation
Electrochemical impedance spectroscopy (EIS)
Seawater corrosion
ATR-FTIR spectroscopy
X-ray photoelectron spectroscopy (XPS)
Passive film stability

ABSTRACT

316L stainless steel is widely used in marine and biomedical applications. However, its protective Cr-rich passive film can be destabilized by microbiologically influenced corrosion (MIC). Here, a multidisciplinary approach combining electrochemical impedance spectroscopy (EIS), potentiodynamic polarization (PP), optical profilometry, ATR-FTIR, X-ray photoelectron spectroscopy (XPS), and ICP-OES was used to investigate corrosion behavior and passive film chemistry of 316L stainless steel (SS) exposed to *Pseudomonas aeruginosa* in artificial seawater, and to evaluate the inhibitory effect of an aqueous *Artemisia annua* extract (AAE).

Exposure to *P. aeruginosa*, resulted in a marked decrease in film resistance, increased corrosion current density, enhanced Fe dissolution, and pronounced surface pitting. Although biotic exposure increased the apparent oxide thickness, XPS analysis revealed the formation of a chemically heterogeneous and less protective surface layer. In contrast, the addition of AAE significantly mitigated these effects by stabilizing a Cr-enriched passive film, increasing charge-transfer resistance, reducing j_{cor}, and suppressing localized attack. ATR-FTIR confirmed adsorption of phenolic acids from AAE, while XPS depth profiling revealed stabilization and thickening of the passive layer. The inhibition efficiency of AAE, evaluated by PP, EIS, and ICP-OES, ranged from 65% to 83%, demonstrating consistent protective behavior across all methods. These results indicate that *A. annua* extract acts as a plant-derived corrosion inhibitor that preserves the functional stability of the Cr-rich passive film under MIC conditions, offering a promising strategy for corrosion mitigation in marine environments.

1. Introduction

Microbiologically influenced corrosion (MIC) remains a persistent challenge in various engineering systems, including marine structures, water systems, energy infrastructure, and biomedical devices. It is estimated that up to 70% of steel corrosion processes are associated with microbial activity, leading to substantial safety, environmental, and economic consequences worldwide [1,2]. Among structural materials, austenitic stainless steels such as 316L are widely employed due to their mechanical robustness and the spontaneous formation of a protective Cr-rich passive film. However, under biofilm covered conditions, microbial metabolism and localized chemical gradients can destabilize this passive layer, promoting chromium depletion, altered oxide chemistry, and accelerated localized corrosion [3,4]. Recent studies have demonstrated that microbiologically induced corrosion of 316L stainless steel may involve intergranular attack, enhanced Fe release, and passive film modification in both marine and biomedical environments [5,6]. Furthermore, comprehensive reviews highlight that interactions between biofilm development and passive film chemistry represent a critical yet insufficiently understood aspect of MIC on stainless steels [7]. Among microorganisms relevant to MIC, *Pseudomonas aeruginosa* is particularly significant due to its ability to form electrochemically active biofilms and modulate interfacial redox processes, thereby influencing the stability and protectiveness of the passive film [3,8].

Current strategies for MIC mitigation frequently rely on toxic biocides and environmentally persistent chemicals, emphasizing the need for sustainable, low toxicity alternatives [9]. In recent years, plant-derived green inhibitors have attracted attention due to their compositions rich in polyphenols, which contain organic molecules capable of adsorbing onto metal surfaces through heteroatoms and

This article is part of a special issue entitled: CCCP published in Hybrid Advances.

* Corresponding author.
E-mail address: gzjelic@fpmoz.sum.ba (G. Zlatić Jelić).

https://doi.org/10.1016/j.hybadv.2026.100639
Received 31 December 2025; Received in revised form 12 February 2026; Accepted 3 March 2026
Available online 5 March 2026

π-electron systems. Beyond simple surface coverage, such compounds may interact with metal oxides, modulate interfacial redox processes, and influence the chemistry and stability of passive films under aggressive conditions [10–12]. By altering surface physicochemical properties, these molecules can also reduce bacterial adhesion and interfere with early biofilm development [12].

Artemisia annua L., a widely distributed medicinal plant rich in phenolic acids, has demonstrated antibacterial and antioxidative activity as well as corrosion inhibition on Fe and Al alloys in simulated seawater [10,13,14]. In our previous work, we developed a simple room-temperature aqueous extraction protocol designed to minimize energy consumption and eliminate organic solvents [13–16]. The resulting aqueous *A. annua* extract (AAE) exhibited high inhibition efficiencies on aluminium alloys in both abiotic and biotic media [14,16] and mitigated corrosion of A36 carbon steel while suppressing *P. aeruginosa* growth in the concentration range 0.50–2.18 mg mL^{-1} [13]. However, the behavior of AAE in systems governed by passive film stability, such as Cr-rich austenitic stainless steels, has not yet been elucidated.

Despite increasing interest in plant derived corrosion inhibitors and MIC of stainless steels, the mechanistic understanding of passive film degradation and stabilization on Cr-rich alloys under biotic conditions remains limited. Previous studies have largely focused on general corrosion metrics, carbon steels, aluminium alloys, or biofilm suppression strategies, with comparatively fewer investigations addressing how biofilm activity alters the chemistry and functional stability of passive films on 316L stainless steel [7,17]. In particular, while increased oxide thickness is often reported under MIC conditions, the relationship between passive film composition, chromium enrichment or depletion, and electrochemical protectiveness remains insufficiently resolved. To address this gap, the present work investigates the behavior of 316L stainless steel exposed to *P. aeruginosa* in artificial seawater and evaluates the influence of an aqueous *A. annua* extract (AAE) using a multimodal approach that integrates electrochemical analysis (EIS and polarization), XPS depth profiling, ATR-FTIR spectroscopy, non-contact optical profilometry, and ICP-OES metal dissolution monitoring. By distinguishing between passive film thickness and functional stability, this study provides mechanistic insight into how a plant derived extract can preserve the Cr-rich oxide layer under MIC conditions. Given the widespread use of 316L in marine and biomedical environments, where corrosion is governed by passivity rather than uniform dissolution, understanding passive film stabilization mechanisms is essential for developing sustainable corrosion mitigation strategies. While the present work focuses on electrochemical and surface-chemical characterization, quantitative microbiological assays and advanced biofilm imaging (e.g., SEM or CLSM) will be required in future studies to further elucidate interactions between the biofilm and inhibitor.

2. Materials and methods

2.1. Substrate conditioning and sterilization protocols

316L stainless steel (20 × 20 × 3 mm) coupons were used as test surfaces for biofilm development. The declared composition of the alloy included (%): 0.020C, 0.500 Si, 0.890 Mn, 0.035 P, <0.001 S, 10.000 Ni, 16.700 Cr, 2.010 Mo, 0.033 N, with Fe comprising the balance. Before exposure to different experimental conditions, samples were mechanically abraded with silicon carbide paper in successive grades (from 360 to 1200 grit), then subjected to ultrasonic cleaning in 96% ethanol for 1 min. Final disinfection was carried out by alternating brief flaming over a Bunsen burner and immersion in 70% ethanol. All procedures were conducted under aseptic conditions.

2.2. Culture medium composition and bacterial inoculation

Pseudomonas aeruginosa ATCC 27853 was re-cultured based on previously described protocols [13–16,18]. For microbial exposure tests, a synthetic analog of seawater (ASWB) was used, with the following composition per liter: 4.1575 g Na_2SO_4, 11.1211 g $MgCl_2{\cdot}6H_2O$, 0.7902 g KCl, 1.5877 g $CaCl_2{\cdot}2H_2O$, 24.9772 g NaCl, 0.0587 g $NaHCO_3$, 5.0000 g peptone, and 1.0000 g yeast extract. Coupons were submerged in either sterile (abiotic) or inoculated (biotic) medium and incubated at 37 °C for intervals of 3, 7, 14, 21, and 30 days. To assess the influence of *Artemisia annua* extract, a parallel set of biotic systems was supplemented with 1 g L^{-1} of the extract (referred to as "inhibited media"), incubated for 14 and 21 days. All bacterial systems were initiated at approcimately10^6 cfu mL^{-1}.

2.3. Extract preparation and application strategy

The aqueous extract of *A. annua* was obtained following the extraction protocol reported in earlier studies [13,14,16,18], using the same batch of plant material as in previous work. Previous phytochemical characterization of this extract revealed that its major phenolic constituents include chlorogenic acid and caffeic acid (Table S1), along with minor flavonoid derivatives, as confirmed by HPLC profiling [16] and ATR-FTIR analysis [13]. These phenolic acids are considered the primary bioactive components responsible for corrosion inhibition. Dried and finely powdered plant material (1.0000 g), collected in southeastern Bosnia and Herzegovina, was immersed in 1 L of ASWB and left to macerate at ambient temperature (25 °C) in the dark. After 3 h, the mixture was filtered using a 0.45 μm filter paper, and the filtrate was adjusted to 1 L with additional ASWB to maintain a consistent composition across tests.

2.4. Electrochemical measurements

Electrochemical measurements were performed using a flat three-electrode cell (Model K0235, Ametek Inc.) with a platinum mesh counter electrode and an Ag | AgCl (3 M KCl) reference electrode. The exposed surface area of the working electrode was 1 cm^2.

Measurements were conducted using an Autolab PGSTAT320 N potentiostat (Metrohm) controlled by Nova 1.5 software. The working electrolyte replicated the ASWB composition without bacterial nutrients (peptone and yeast extract).

Open circuit potential (E_{OCP}), electrochemical impedance spectroscopy (EIS), and potentiodynamic polarization (PP) were employed to evaluate corrosion behavior. EIS measurements were carried out at E_{OCP} using a 10 mV rms AC perturbation over a frequency range from 10 kHz to 5 mHz. Polarization scans were performed within ±200 mV vs. E_{OCP} at a scan rate of 0.5 mV s^{-1} [18].

All electrochemical measurements were repeated on independently prepared electrodes to confirm reproducibility. Only stable and representative spectra and polarization curves corresponding to steady-state conditions are presented.

2.5. Surface film analysis

Coupons exposed to different media (abiotic, biotic, inhibited) were abundantly and gently rinsed with ASWB, then dehydrated using an ethanol gradient (25-96%), after which oxide layers formed on 316L coupons were examined using complementary analytical techniques [18]. Independent experiments were performed to confirm reproducibility of surface analytical results. Representative data sets are reported.

2.5.1. Topographical imaging by optical profilometry

Surface morphology and roughness were analyzed using a non-contact profilometer (ZYGO NewView 7100, Zygo Corporation, USA). Measurements were standardized to a 1.092 × 1.092 mm^2 area across all samples.

2.5.2. Elemental and chemical profiling via XPS

X-ray photoelectron spectroscopy (XPS) analyses were performed using a PHI-TFA XPS system (Physical Electronics, USA) equipped with a monochromatic Al Kα source. The probed surface area was 0.4 mm in diameter with an energy resolution of ±0.3 eV. Survey spectra were acquired from a representative region of each sample and quantified using standard sensitivity factors [19], atomic percentages are therefore reported as representative values intended for comparative analysis between conditions. Depth profiling was achieved by Ar-ion sputtering (1 keV, ~0.8 nm/min), enabling analysis of the oxide layers down to a few nanometers.

2.5.3. Molecular fingerprinting using ATR-FTIR

ATR-FTIR spectra were recorded using an IRAffinity-1S spectrometer (Shimadzu, Japan) equipped with a GladiATR10 accessory. Spectra were collected directly from dehydrated 316L surfaces after 14 days of incubation in different media.

For comparison, an ATR-FTIR spectrum of a solid caffeic acid standard (Sigma-Aldrich, ≥98%) was recorded under identical conditions to support band assignment and confirm the presence of phenolic acids derived from the extract.

2.5.4. Quantification of dissolved metals using ICP-OES

The elemental composition of alloying elements following short-term (1 h) immersion of exposed 316L electrodes in absolute ethanol for dissolution of released metal species was analyzed via ICP-OES (iCAP 6500 Duo, Thermo Scientific, UK). After immersion, the ethanol was evaporated to 1 mL and diluted to 10 mL with ultrapure water. Concentrations of Fe, Cr, Mn, Mo and Ni were quantified using calibration curves derived from certified multi-element standards (Alfa Aesar, Specture®; VHG Labs, EPA Method Standard).

2.6. Estimation of inhibitory efficiency of A. annua

The efficiency of *A. annua* extract (AAE) in mitigating microbiologically influenced corrosion (MIC) on 316L was quantified from electrochemical data. From EIS, inhibition efficiency (IE) was calculated using polarization resistance values extrapolated at low frequency:

$$IE\ (\%) = \frac{R'_P - R_P}{R'_P} \times 100 \quad (1)$$

where R_p denotes resistance in an extract-free medium, and R'_p stands for inhibited medium [16]. Similarly, from PP curves, *IE* was determined via corrosion current densities:

$$IE(\%) = \frac{j^0_{cor} - j_{cor}}{j^0_{cor}} \times 100 \quad (2)$$

Here, j^0_{cor} and j_{cor} are the current densities in the absence and presence of AAE, respectively [20]. The assessment of inhibitory efficiency was also calculated from ICP-OES results using Equations (3) and (4). First, the corrosion rate of 316L SS was calculated by applying Equation (3):

$$r_{cor} = \frac{W}{At} \quad (3)$$

In this equation, *W* denotes the amount of iron released (in μg), *A* refers to the exposed surface area of the working electrode (4 cm^2), and *t* represents the immersion time in hours (t = 1 h) [21,22]. To assess the efficiency of *Artemisia annua* aqueous extract in reducing the corrosion induced by *Pseudomonas aeruginosa*, the inhibition efficiency (*IE*) was calculated using Equation (4):

$$IE(\%) = \frac{r^0_{cor} - r_{cor}}{r^0_{cor}} \times 100 \quad (4)$$

Here, r^0_{cor} denotes the rate in the biotic medium, while r_{cor} corresponds to the corrosion rate measured in the presence of the extract (inhibited medium) [22].

3. Results and discussion

3.1. Electrochemical results

3.1.1. Electrochemical impedance spectroscopy

Electrochemical impedance spectroscopy (EIS) was used to evaluate the corrosion behavior of 316L stainless steel in artificial seawater following incubation in abiotic and biotic media.

Nyquist and Bode plots recorded after 3, 7, and 30 days (Figs. 1 and 2) reveal a progressive increase in total system impedance with immersion time. However, samples incubated in the biotic medium consistently exhibited lower impedance than those in the abiotic medium indicating a diminished barrier effect in the presence of *P. aeruginosa*. EIS spectra were fitted using the equivalent electrical circuits (EECs) shown in Fig. 3.

Samples exposed to the abiotic medium and those incubated in the biotic medium for 3 days were described by the two-time-constant model [*R* (Q_1 [R_1 (Q_2R_2)])] (Fig. 3a), which reflects a surface/passive film response (Q_1, R_1) coupled with a charge-transfer process at the metal/film interface (Q_2, R_2). In contrast, biotic samples at 7 and 30 days were better represented by the model [*R* (Q_1R_1) (Q_2R_2)] (Fig. 3b), suggesting modification of interfacial processes, likely associated with

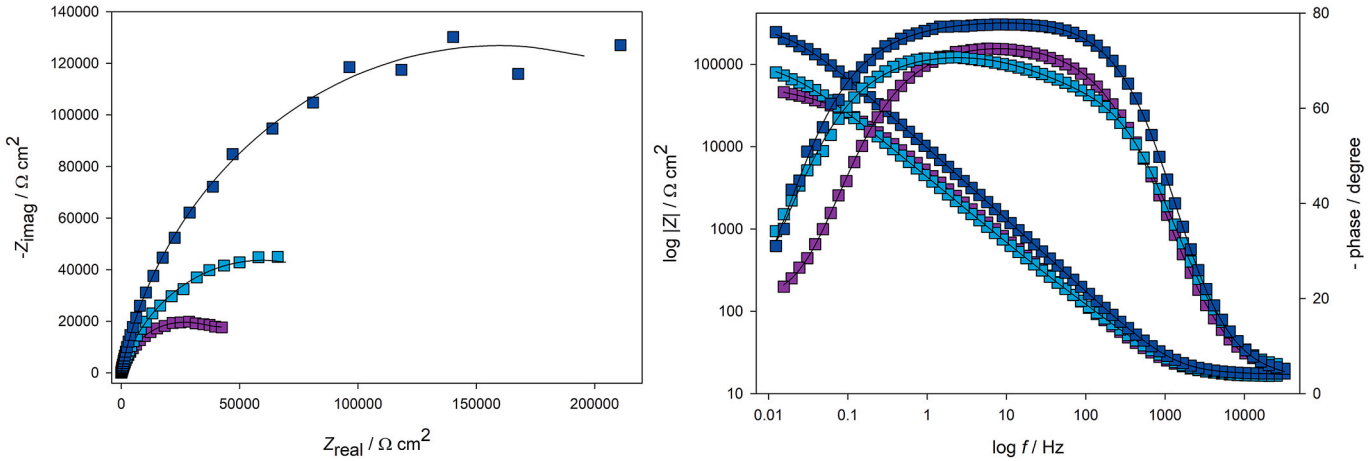

Fig. 1. Nyquist and Bode plots of impedance spectra of 316L SS recorded in artificial sweater after incubation in abiotic (■3 d; ■7 d; ■30 d — fitted curves) media.

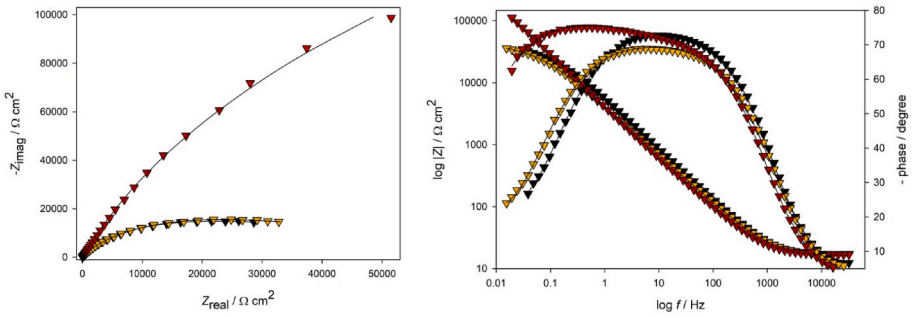

Fig. 2. Nyquist and Bode plots of impedance spectra of 316L SS recorded in artificial sweater after incubation in biotic (▼3 d; ▼7 d; ▼30 d; — fitted curves) media.

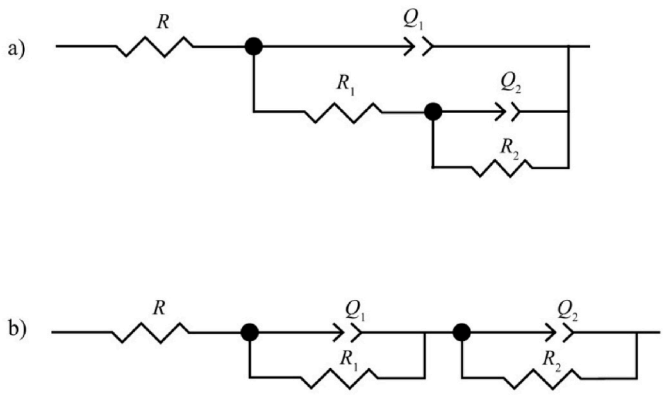

Fig. 3. The equivalent electrical circuits used in modeling the impedance spectra shown in Figs. 1–2 and 4.

Table 1
Values of EEC elements obtained by analyzing the impedance spectra of the 316L steel electrode from Figs. 1 and 2.

Media	t	$Q_1 \times 10^5$	n_1	R_1	$Q_2 \times 10^5$	n_2	R_2
	d	$\Omega^{-1}s^n$ cm^{-2}		kΩ cm^2	$\Omega^{-1}s^n$ cm^{-2}		kΩ cm^2
Abiotic	3	4.26	0.828	21.04	12.61	0.986	22.54
	7	3.65	0.833	26.01	1.64	0.943	43.73
	30	4.67	0.828	57.23	1.64	0.970	139.88
Biotic	3	3.62	0.834	9.67	17.14	0.917	18.95
	7	5.46	0.792	10.19	15.40	0.908	22.68
	30	5.06	0.706	12.01	55.25	0.858	36.31

biofilm development and increased surface heterogeneity. The fitted parameters are summarized in Table 1.

Under abiotic conditions, the resistance of the surface film (R_1) increased from 21.0 kΩ cm^2 to 57.2 kΩ cm^2, over 30 days, while the charge transfer resistance (R_2) rose from 22.5 kΩ cm^2 to 139.9 kΩ cm^2. This progressive increase in both parameters indicates enhanced barrier properties and improved electrochemical stability of the Cr-rich passive film during immersion [23]. In the biotic medium, however, both R_1 and R_2 remained significantly lower throughout the same exposure period. After 30 days, the R_2 value (36.3 kΩ cm^2) was nearly fourfold lower than in the corresponding abiotic system, reflecting accelerated interfacial charge transfer and reduced functional stability of the passive layer in the presence of *P. aeruginosa*. The lower R_1 values further suggest that although an oxide layer persists, its protective integrity is compromised under biofilm covered conditions. In addition, the decrease in n values under biotic conditions (Table 1) indicates increased surface heterogeneity and deviation from ideal capacitive behavior, consistent with biofilm coverage and chemical inhomogeneity of the passive layer.

The influence of *Artemisia annua* extract (AAE) on film formation in the presence of *P. aeruginosa* after 14 days is shown in Fig. 4. The open circuit potentials (E_{OCP}) were −0.085 V for the abiotic medium, −0.037 V for the biotic medium, and −0.224 V for the inhibited medium. EIS data for the abiotic and inhibited conditions were described by [R (Q_1 [R_1 (Q_2R_2)])] (Fig. 3a), whereas spectra collected in the biotic medium required [R (Q_1R_1) (Q_2R_2)] (Fig. 3b) for accurate representation [24]. The electrolyte resistance remained constant at 17.4 Ω cm^2 across all measurements, and EEC fitting results are summarized in Table 2.

The negative effect of *P. aeruginosa* on the development of passive film is evident from the strong reduction in R_1, with the biotic film exhibiting a resistance of only 2.45 kΩ cm^2, which is sixteen- and fourteen-fold lower than in the abiotic (39.2 kΩ cm^2) and inhibited (35.3 kΩ cm^2) media, respectively. This substantial decline indicates disruption and increased heterogeneity of the passive film rather than its complete absence. Importantly, the addition of AAE to the biotic medium markedly enhanced charge transfer resistance, increasing R_2 to 63.8 kΩ cm^2, which is approximately twice the value observed for the uninhibited biotic system (32.5 kΩ cm^2) under identical incubation

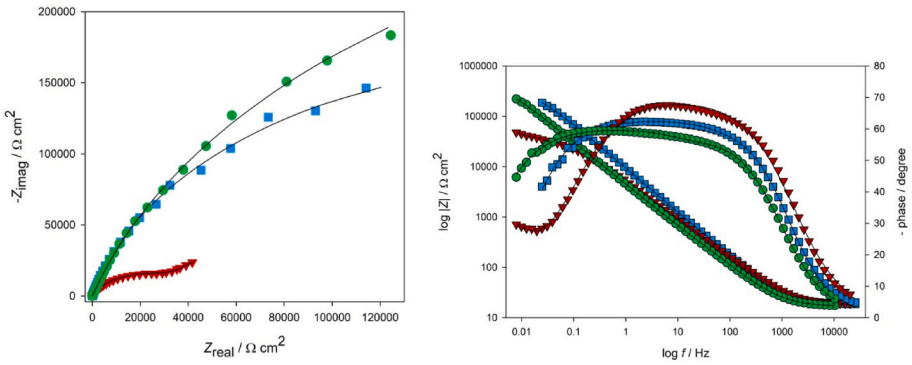

Fig. 4. Nyquist and Bode plots of impedance spectra recorded on a 316L steel electrode in artificial seawater solution after incubation in abiotic (■), biotic (▼). and inhibited (●) media for 14 days. The lines show the modeled data.

Table 2
Values of EEC elements obtained by analyzing the impedance spectra of the 316L steel electrode from Fig. 4.

Medium	$Q_1 \times 10^5$	n_1	R_1	$Q_2 \times 10^5$	n_2	R_2
	Ω^{-1} s^n cm^{-2}		kΩ cm^2	Ω^{-1} s^n cm^{-2}		kΩ cm^2
Abiotic	2.85	0.873	39.20	4.40	0.963	123.40
Biotic	4.49	0.773	2.45	48.98	0.802	32.49
Inhibited	4.26	0.835	35.34	0.81	0.985	63.80

conditions (Table 2). Similar increases in charge-transfer resistance during MIC mitigation of stainless steels have been reported for D-cysteine-modified systems [17], where inhibition was attributed to suppression of biofilm induced passive film destabilization.

Overall, EIS results demonstrate that *P. aeruginosa* compromises the functional stability of the passive film on 316L stainless steel, leading to reduced barrier resistance and enhanced charge transfer. In contrast, the presence of AAE partially restores electrochemical resistance by stabilizing the surface film and suppressing corrosion kinetics. This behavior is consistent with adsorption of phenolic compounds, such as chlorogenic and caffeic acid [16], which may interact with surface oxides and reinforce the protective Cr-rich passive layer under microbiologically influenced conditions.

3.1.2. Potentiodynamic polarization

Polarization curves recorded for 316L stainless steel in artificial seawater after 14 days of incubation in abiotic, biotic, and inhibited media are presented in Fig. 5. The corrosion parameters derived from these experimental curves are summarized in Table 3.

As shown in Table 3, the highest corrosion current density of 0.217 µA cm^{-2} was observed for electrodes incubated in the biotic medium, whereas the lowest value, 0.044 µA cm^{-2}, was obtained in the inhibited medium, closely matching the abiotic condition (0.058 µA cm^{-2}). The pronounced increase in j_{cor} under biotic conditions (Fig. 5, Table 3) confirms that *P. aeruginosa* accelerates the corrosion of 316L stainless steel most likely through biofilm mediated destabilization of the passive Cr-rich oxide layer and modification of interfacial electrochemical reactions. The corrosion potential (E_{cor}) also shifted positively in the biotic system (−0.124 V) relative to the abiotic condition (−0.190 V), suggesting altered anodic-cathodic balance in the presence of metabolically active bacteria. The observed increase in corrosion current density under biotic conditions aligns with previously reported MIC acceleration of 316L in saliva and marine analogues [5,6]. In contrast, the inhibited system exhibited a more negative E_{cor} (−0.248 V), consistent with partial suppression of anodic dissolution processes and stabilization of the passive film.

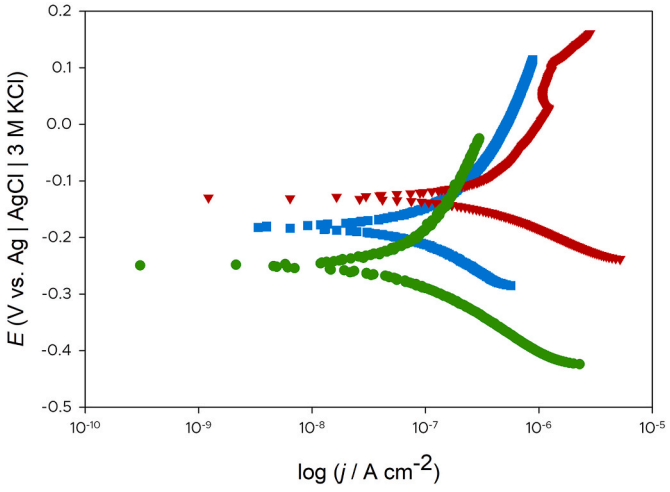

Fig. 5. Polarization curves of 316L stainless steel in artificial seawater after 14 days of incubation in abiotic (■), biotic (▼). and inhibited (●) media, recorded at a potential scan rate of $\nu = 0.5$ mV s^{-1}.

Table 3
Corrosion parameters for 316L stainless steel in artificial seawater after 14 days of incubation in abiotic, biotic, and inhibited media, obtained from analysis of the experimental results shown in Fig. 5.

Media	b_a	b_c	E_{cor}	j_{cor}
	V dec^{-1}	V dec^{-1}	V	µA cm^{-2}
Abiotic	0.112	0.124	−0.190	0.058
Biotic	0.091	0.141	−0.124	0.217
Inhibited	0.103	0.179	−0.248	0.044

The addition of AAE resulted in a substantial reduction in j_{cor}, corresponding to an inhibition efficiency of approximately 80% relative to the uninhibited biotic condition. The moderate changes in both anodic (b_a) and cathodic (b_c) Tafel slopes indicate that AAE influences both partial reactions, suggesting a mixed-type inhibition mechanism rather than purely anodic or cathodic control. The corresponding inhibition efficiencies calculated from electrochemical data are summarized separately in Table 6 for clarity.

The polarization results corroborate the EIS findings, demonstrating that *P. aeruginosa* compromises protection attained from passive film, whereas AAE partially restores electrochemical stability. Importantly, while polarization measurements quantify corrosion kinetics, the concurrent increase in R_2 observed in EIS confirms that the improvement is associated with enhanced charge transfer resistance and not merely a shift in corrosion potential. These complementary techniques therefore support the interpretation that AAE preserves the functional integrity of the Cr-rich passive film under MIC conditions.

3.2. Optical profilometry

The results of the profilometric analysis of 316L stainless steel electrodes exposed to abiotic, biotic, and inhibited media for 21 days are shown in Figs. 6–8.

The three-dimensional (3D) and linear (2D) surface profiles of electrodes incubated in the biotic medium reveal clear signs of localized pitting damage (Fig. 7). The maximum pit depth observed in the 2D profile reached approximately 1.25 µm. Such damage was not observed on electrodes exposed to the abiotic medium (Fig. 6) nor on those incubated in the inhibited medium (Fig. 8). The average surface roughness of the film formed on electrodes incubated in the biotic medium was approximately 0.108 µm. In contrast, electrodes exposed to the abiotic medium exhibited only a few shallow pits and developed a surface film with an average roughness of ~0.086 µm (Fig. 6). Similar behavior was observed when *Artemisia annua* extract was added to the biotic medium: the number of pits was substantially reduced, and a more uniform surface film formed, with an average roughness of ~0.099 µm (Fig. 7) [25].

3.3. XPS surface and depth profiling

X-ray photoelectron spectroscopy (XPS) was employed to characterize the chemical composition and oxidation states of the oxide films formed on 316L stainless steel electrodes after 14-day incubation in abiotic, biotic, and inhibited media. Additionally, argon ion sputtering combined with depth profiling was used to examine the elemental distribution within the surface layer and estimate oxide thicknesses.

Survey XPS spectra (Figs. S1–S3) revealed the presence of Fe, Cr, Ni, O, C, N, P, Ca, and Na across all samples, reflecting contributions from both the native passive film and species derived from the electrolyte and biological environment. Quantitative surface compositions derived from representative survey spectra are summarized in Table 4 and are discussed comparatively across conditions.

High-resolution Cr $2p_{3/2}$ spectra (Fig. 9a–c) displayed three peaks:

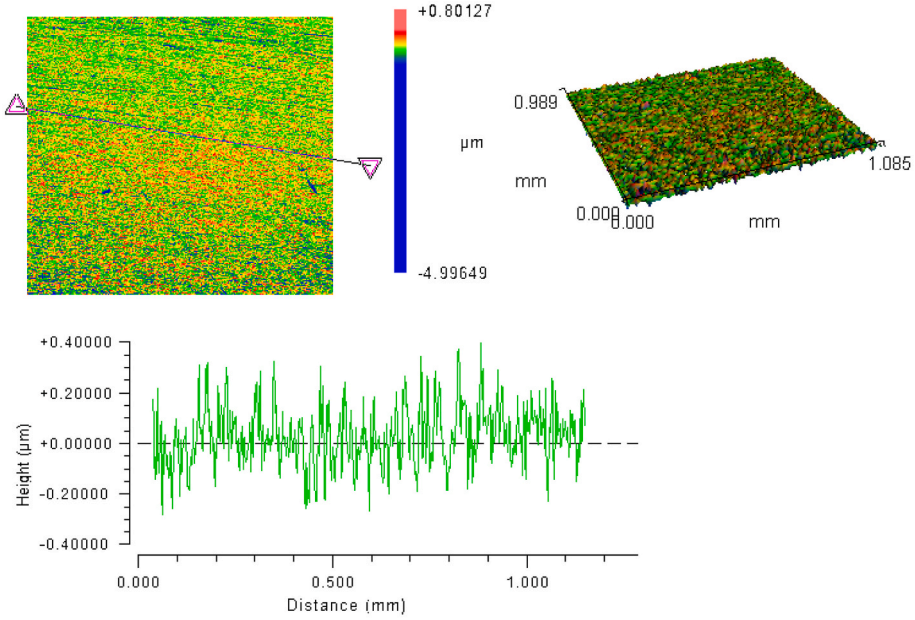

Fig. 6. 2D and 3D profiles of the 316L SS surface exposed to an abiotic medium for 21 days.

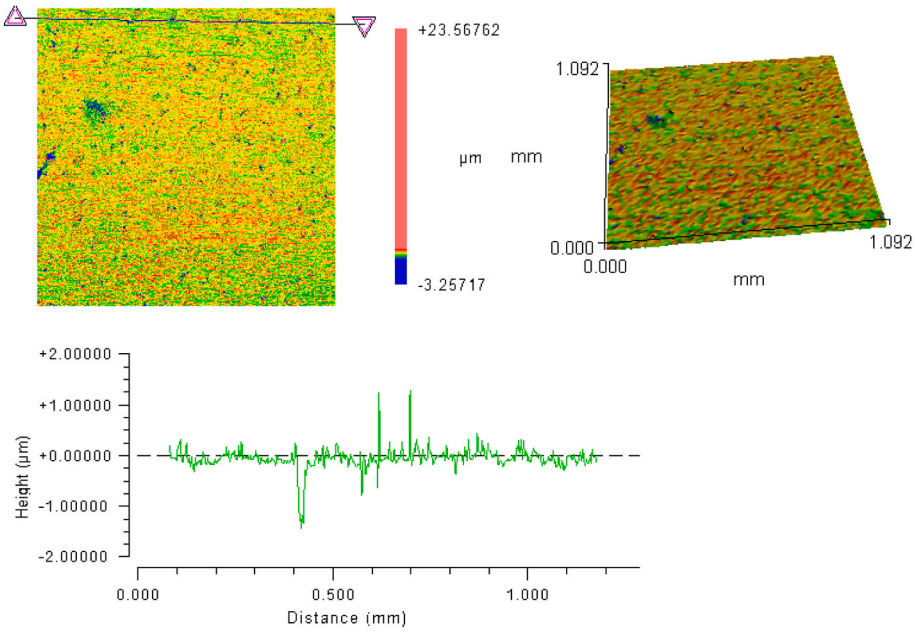

Fig. 7. 2D and 3D profiles of the 316L SS surface exposed to biotic medium for 21 days.

metallic Cr^0 at ~575.0 eV, Cr^{3+} at ~576.7 eV, and a Cr-plasmon shoulder at ~578.0 eV. The spectral shapes were consistent across all media, suggesting a thin Cr_2O_3-type oxide on the Fe–Cr substrate [26]. However, subtle differences in relative intensities and surface atomic ratios indicate that the chemical stability of this layer is influenced by the incubation environment.

Depth profiling up to 20 nm (Fig. 10) revealed a surface-enriched oxide layer composed primarily of Cr and Fe oxides in all cases. The estimated oxide thicknesses were 2.5 ± 0.5 nm (abiotic), 3.0 ± 0.5 nm (biotic), and 4.0 ± 0.5 nm (inhibited). Notably thicker oxide layer was observed under biotic conditions, compared to abiotic sample that exhibited the thinnest film. This trend demonstrates that oxide thickness alone does not directly correlate with electrochemical corrosion resistance. Despite its greater thickness, the biotic film exhibited significantly lower charge-transfer resistance (R_2) and higher corrosion current density (j_{cor}), indicating that microbial activity promotes the formation of a chemically less stable and more defective oxide.

In contrast, the inhibited sample displayed both increased thickness and improved electrochemical resistance. The enhanced Cr/Fe surface ratio observed in Table 4 suggests that AAE promotes stabilization of the Cr-rich component of the passive layer rather than merely increasing overall oxide growth. Preservation of chromium enrichment is particularly important for 316L stainless steel, as corrosion resistance is governed by the integrity of the Cr_2O_3-based passive film rather than by

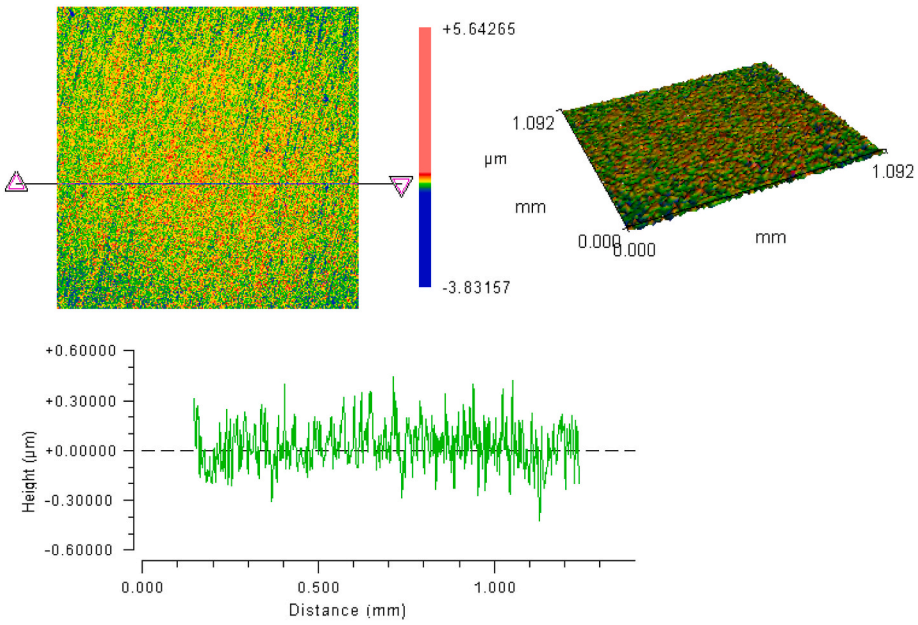

Fig. 8. 2D and 3D profiles of the 316L SS surface exposed to an inhibited medium for 21 days.

Table 4
Quantitative composition of the 316L SS surfaces after 14 days of incubation in abiotic, biotic and inhibited media calculated from the XPS spectra shown in Figs. S1–S3 (expressed in at.%).

Medium	Element						
	C	O	N	P	Ca	Cr	Fe
Abiotic	50.2	37.3	3.7	3.1	1.8	2.6	1.3
Biotic	47.9	37.1	5.0	2.9	2.3	3.0	1.8
Inhibited	52.9	34.9	4.3	3.0	2.6	1.6	0.7

total oxide thickness. These findings are consistent with reports that MIC on Cr-containing stainless steels promotes Fe enrichment and Cr depletion of the passive layer [6,7].

The higher surface carbon content detected for the inhibited sample relative to the biotic condition is consistent with the adsorption of phenolic acids onto the steel surface. The combined XPS and electrochemical data therefore indicate a multimodal inhibition mechanism: microbial activity disrupts passive-film chemistry and increases heterogeneity, whereas AAE stabilizes the Cr-rich oxide and suppresses charge-transfer reactions without simply producing a thicker but less protective film.

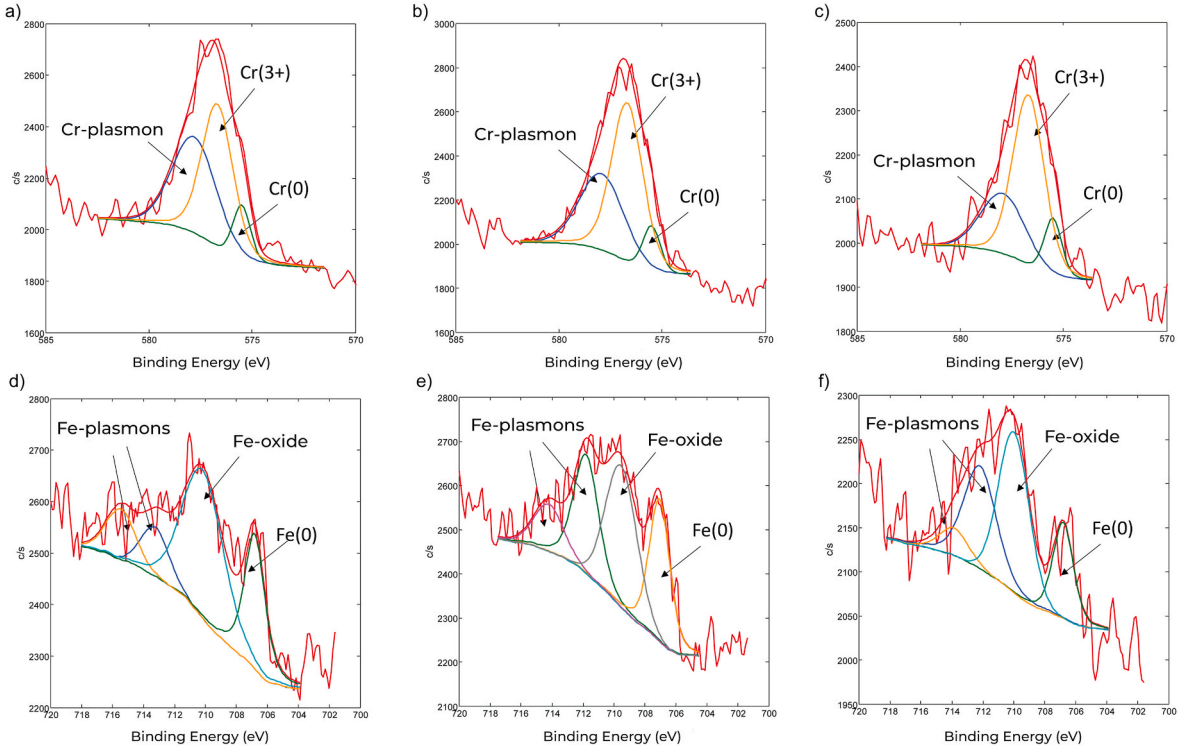

Fig. 9. Normalized high-resolution Cr $2p_{3/2}$ (a, b, c) and Fe $2p_{3/2}$ (d, e, f) XPS spectra of 316L stainless steel incubated in the abiotic (a, d), biotic (b, e), and inhibited media (c, f).

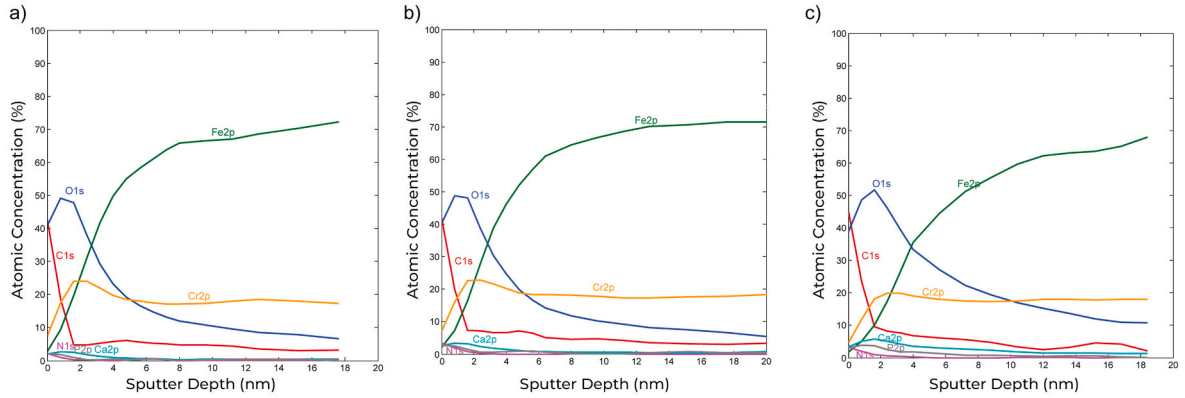

Fig. 10. XPS depth-profile elemental distributions for 316L stainless steel electrodes incubated in the abiotic (a), biotic (b), and inhibited media (c).

3.4. ATR-FTIR spectroscopy

ATR-FTIR spectra of the 316L stainless steel surfaces recorded after 14 days of incubation in biotic and inhibited media are presented in Fig. 11.

The spectrum of the electrode incubated in the biotic medium exhibits a characteristic broad band in the region between 700 and 400 cm^{-1}, which is associated with Fe–O and Fe–O–H vibrational modes characteristic of iron (III) hydroxides and oxyhydroxides [27]. The presence of an –OH stretching band centered at approximately 3240 cm^{-1} further supports the formation of hydrated Fe(III) oxyhydroxide species on the steel surface [28]. These features are consistent with the XPS results, which indicate increased iron oxide contributions under biotic conditions, and with the elevated corrosion current density measured by polarization analysis.

In addition, two prominent bands observed near 1600 cm^{-1} and 1100 cm^{-1} are attributed to vibrations of carboxyl-containing functional groups and polysaccharide-related stretching modes, respectively [13,29–31]. These signatures are characteristic of extracellular polymeric substances (EPS), supporting the development of a biofilm layer on the steel surface. The increased nitrogen content detected by XPS (Table 4) under biotic conditions further corroborates the presence of biologically derived surface species.

In contrast, the ATR-FTIR spectrum of the steel electrode incubated in the inhibited medium shows distinct bands at approximately 1640 cm^{-1} and 1520 cm^{-1}, which are assigned to the asymmetric and symmetric stretching vibrations of the deprotonated carboxylate group (COO^{-}), respectively [14,32,33]. These bands closely resemble those reported in the previously published ATR-FTIR spectrum of the aqeous *Artemisia annua* L. extract [14] in which phenolic acids were identified as major constituents. HPLC analysis of AAE [16,33,34] confirmed the presence of chlorogenic acid and caffeic acid as dominant phenolic components, supporting the assignment of these vibrational features to adsorbed phenolic species.[35]

To further validate this interpretation, the ATR-FTIR spectrum of pure caffeic acid standard recorded in the solid state is presented in Fig. 12. The spectrum exhibits broad O–H stretching in the 3400–3200 cm^{-1} region and characteristic bands near 1600, 1440, and 1270–1100 cm^{-1} [36,37]. The overlap of these features with those observed on the inhibited steel surface (Fig. 11), together with prior HPLC profiling [16] and the reported ATR-FTIR spectrum of AAE [14], supports the presence of adsorbed phenolic constituents from the extract. In view of the complex interfacial environment, this evidence is interpreted as indicative of adsorption rather than specific chemical bonding.[35]

The absence of significant attenuation of biofilm-related bands in the inhibited spectrum, combined with the appearance of phenolic signatures, indicates that AAE components competitively adsorb onto the steel surface, modifying the interfacial chemistry and suppressing EPS accumulation. This interpretation is consistent with the improved charge transfer resistance observed in EIS measurements, reduced corrosion current density in polarization experiments, and enhanced Cr/Fe surface ratio detected by XPS.

Taken together, the FTIR, XPS, and electrochemical results support a multimodal inhibition mechanism in which phenolic compounds of AAE

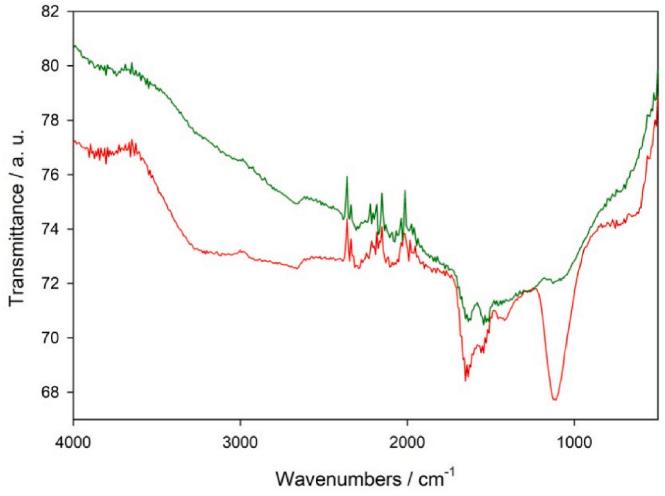

Fig. 11. ATR-FTIR spectra of the 316L SS surfaces that were incubated in biotic (red) and inhibited media (green) for 14 days.

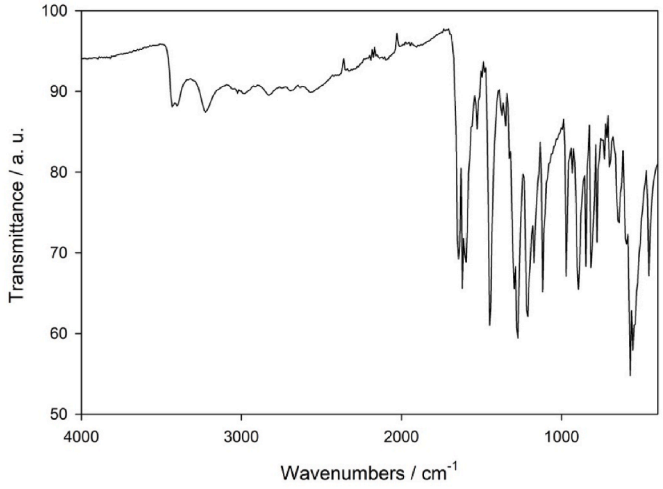

Fig. 12. ATR-FTIR spectrum of caffeic acid standard.

adsorb onto active surface sites, limit Fe dissolution, and preserve the integrity of the Cr-rich passive film under microbiologically influenced corrosion conditions.

3.5. ICP-OES

The concentrations of Fe, Cr, Mn, Mo, and Ni released from the 316L stainless steel electrodes after short-term immersion tests were quantified by inductively coupled plasma optical emission spectroscopy (ICP-OES) and are summarized in Table 5.

Iron dissolution was markedly reduced in the presence of *Artemisia annua* extract. The Fe concentration decreased from $74.8 \pm 1.0\,\mu g\,L^{-1}$ cm^{-2} in the biotic medium to $12.5 \pm 0.3\,\mu g\,L^{-1}$ cm^{-2} in the inhibited system, corresponding to an approximately six fold reduction. This substantial decrease confirms that AAE effectively suppresses Fe release, which represents the dominant dissolution pathway under microbiologically influenced corrosion conditions.

Chromium release showed only a minor decrease (3.8 ± 0.2 to $3.4 \pm 0.2\,\mu g\,L^{-1}$ cm^{-2}), indicating that the Cr-rich passive component remained relatively stable in both environments. The preferential reduction of Fe dissolution in the inhibited medium is consistent with XPS results showing enhanced Cr/Fe surface ratios and with electrochemical measurements demonstrating increased charge transfer resistance. Similar decreasing trends were observed for Mo and Ni, while Mn exhibited a slight increase under inhibited conditions, likely reflecting redistribution processes within the alloy rather than accelerated corrosion.

Using the quantified Fe release, the corrosion rate was calculated according to Equation (3). The corrosion rate decreased proportionally with Fe concentration in the inhibited medium (Table 5), confirming that the reduction in electrochemical activity observed by polarization and impedance measurements corresponds to a measurable decrease in cumulative metal dissolution. These results provide independent chemical evidence that AAE mitigates MIC degradation of 316L stainless steel.

3.6. Inhibition efficiency

The inhibition efficiency (*IE*) of *A. annua* aqueous extract against MIC-induced corrosion of 316L SS was evaluated using three independent techniques: electrochemical impedance spectroscopy (EIS), potentiodynamic polarization, and ICP-OES analysis of dissolved Fe (Table 6).

The calculated IE values were approximately 65% (EIS), 80% (PP), and 83% (ICP-OES). Although the IE deduced from EIS data is slightly lower, such variation is expected due to methodological differences. EIS primarily reflects interfacial resistance and integrity of the passive film, whereas polarization analysis quantifies corrosion kinetics, and ICP-OES measures cumulative metal dissolution. The higher IE derived from ICP-OES indicates that AAE substantially suppresses total Fe release, while the EIS value reflects partial but significant restoration of protective properties of passive film under biotic conditions. All three techniques consistently confirm strong inhibition of MIC on 316L stainless steel by AAE.

From a mechanistic perspective, the results support a stepwise inhibition. Under biotic conditions, *P. aeruginosa* biofilm formation and associated extracellular polymeric substances promote passive film destabilization, increase interfacial heterogeneity (as reflected by reduced *n*-values), decrease charge transfer resistance, and increased Fe dissolution. XPS and ICP-OES data confirm preferential Fe release and the formation of a chemically less protective, Fe-enriched oxide layer, despite modest increases in total oxide thickness. In contrast, in the presence of AAE, phenolic compounds adsorb onto the steel surface, competitively modifying the interfacial chemistry and attenuating biofilm associated signatures. This adsorption correlates with preservation of Cr enrichment within the passive layer, increased charge-transfer resistance, and a substantial reduction in Fe release.

Taken together, the combined EIS, PP, FTIR, XPS, profilometry, and ICP-OES data indicate that AAE functions as an interfacial modifier that stabilizes the Cr-rich passive film, suppresses microbiologically induced Fe dissolution, and mitigates MIC degradation without relying solely on increased oxide thickness.

Table 6
Inhibition efficiency (*IE*) of *A. annua* aqueous extract against MIC-induced corrosion of 316L stainless steel, determined by electrochemical impedance spectroscopy, EIS (using Equation (1)) potentiodynamic polarization, PP (using Equation (2)), and ICP-OES quantification of dissolved Fe (using Equations (3) and (4)).

Method	*IE* (%)
EIS	64.7
PP	79.7
ICP-OES	83.3

4. Conclusion

The integrated electrochemical, spectroscopic, and surface analyses demonstrate that *P. aeruginosa* significantly destabilizes the passive film on 316L stainless steel in artificial seawater, leading to increased surface heterogeneity, reduced charge transfer resistance, increased corrosion current density, Fe dissolution, and localized pitting. Although oxide thickness under biotic conditions was not reduced, the combined EIS, polarization, XPS, and ICP-OES data reveal that the biofilm promotes the formation of a chemically less protective and Fe-enriched surface layer, thereby destabilizing passive film.

In contrast, the addition of *A. annua* aqueous extract effectively mitigated MIC. AAE reduced Fe dissolution, restored charge transfer resistance, suppressed biofilm formation and preserved chromium enrichment within the passive layer. ATR-FTIR confirmed adsorption of phenolic compounds, while XPS depth profiling demonstrated stabilization of the Cr-rich oxide rather than simple thickening of the surface film. Together, these findings support a multimodal inhibition mechanism in which AAE acts as an interfacial modifier that stabilizes passive film chemistry and limits MIC of 316L stainless steel, highlighting the potential of plant derived extracts as sustainable corrosion mitigation strategies for alloys used in marine and biomedical environments. Although AAE represents a solvent-free, plant-derived candidate with low expected toxicity, comprehensive toxicological and biodegradability assessments are required prior to large scale or field application.

Table 5
Concentrations of elements released after short immersion tests of treated 316L steel electrodes measured by ICP-OES.

Media	Element ($\mu g\,L^{-1}$ cm^{-2})					r_{cor} ($\mu g\,cm^{-2}\,h^{-1}$)
	Fe	Cr	Mn	Mo	Ni	
Biotic	74.8 ± 1.0	3.8 ± 0.2	4.3 ± 0.2	6.4 ± 0.2	3.7 ± 0.2	0.75 ± 0.01
Inhibited	12.5 ± 0.3	3.4 ± 0.2	6.3 ± 0.5	0.8 ± 0.1	2.5 ± 0.1	0.125 ± 0.003

Data availability statement

Data available on request.

CRediT authorship contribution statement

Gloria Zlatić Jelić: Conceptualization, Data curation, Formal analysis, Investigation, Methodology, Resources, Software, Validation, Visualization, Writing – original draft, Writing – review & editing. **Ivana Martinović:** Funding acquisition, Project administration, Resources, Supervision, Validation, Writing – review & editing. **Zora Pilić:** Funding acquisition, Project administration, Resources, Supervision, Writing – review & editing. **Janez Kovač:** Formal analysis, Project administration, Resources. **Marcela Romić:** Resources, Validation.

Declaration of competing interest

The authors declare that they have no known competing financial interests or personal relationships that could have appeared to influence the work reported in this paper.

Acknowledgments

The authors would like to acknowledge the financial support for the conduct of the research received from the Federal Ministry of Education and Science, Bosnia and Herzegovina. This work was also supported by the Slovenian Research Agency (Programme P2-0082).

Appendix A. Supplementary data

Supplementary data to this article can be found online at https://doi.org/10.1016/j.hybadv.2026.100639.

References

[1] Y. Jin, Z. Li, E. Zhou, Y. Lekbach, D. Xu, S. Jiang, F. Wang, Sharing riboflavin as an electron shuttle enhances the corrosivity of a mixed consortium of Shewanella oneidensis and Bacillus licheniformis against 316L stainless steel, Electrochim. Acta 316 (2019) 93, https://doi.org/10.1016/j.electacta.2019.05.094.

[2] M. Lv, M. Du, A review: microbiologically influenced corrosion and the effect of cathodic polarization on typical bacteria, Rev. Environ. Sci. Biotechnol. 17 (2018) 431, https://doi.org/10.1007/s11157-018-9473-2.

[3] Yi Yang, Enze Zhou, Lingke Li, Xuqin Peng, Ye Huang, Chengying Jiang, Tingyue Gu, Fuhui Wang, Dake Xu, The role of phenazines in marine Pseudomonas aeruginosa microbiologically influenced corrosion against 316L stainless, steel Corrosion Science 242 (2025) 112587, https://doi.org/10.1016/j.corsci.2024.112587.

[4] Z. Li, Y. Chen, Q. Guo, X. Zhang, X. Li, Y. Li, J. Cai, Y. Fan, J. Yang, A comparative evaluation of microbiologically induced corrosion behaviors of 316L austenitic and 2205 duplex stainless steels inoculated in Desulfovibrio vulgaris, Metals 15 (9) (2025) 1040, https://doi.org/10.3390/met15091040.

[5] Padmalatha Rao, Lavanya Mulky, An overview of microbiologically influenced corrosion on stainless steel, ChemBioEng Rev. 10 (2023) 829–840, https://doi.org/10.1002/cben.202300001.

[6] Ubong Eduok, Microbiologically induced intergranular corrosion of 316L stainless steel dental material in saliva, Mater. Chem. Phys. 313 (2024) 128799, https://doi.org/10.1016/j.matchemphys.2023.128799.

[7] Koena Maji, M. Lavanya, Microbiologically influenced corrosion in stainless steel by pseudomonas aeruginosa: an overview, J. Bio Tribo Corros. 10 (2024) 16, https://doi.org/10.1007/s40735-024-00820-w.

[8] K.A. Mielko, S.J. Jabłoński, J. Milczewska, D. Sands, M. Łukaszewicz, P. Młynarz, Metabolomic studies of Pseudomonas aeruginosa, World J. Microbiol. Biotechnol. 35 (2019) 178, https://doi.org/10.1007/s11274-019-2739-1.

[9] I. Amara, W. Miled, R. Ben Slama, N. Ladhari, Antifouling processes and toxicity effects of antifouling paints on marine environment. A review, Environ. Toxicol. Pharmacol. 57 (2018) 115–130.

[10] A. Septembre-Malaterre, M. Lalarizo Rakoto, C. Marodon, Y. Bedoui, J. Nakab, E. Simon, L. Hoarau, S. Savriama, D. Strasberg, P. Guiraud, et al., Artemisia annua, a traditional plant brought to light, Int. J. Mol. Sci. 21 (14) (2020) 4986, https://doi.org/10.3390/ijms21144986.

[11] L. Othman, A. Sleiman, R.M. Abdel-Massih, Antimicrobial activity of polyphenols and alkaloids in Middle Eastern plants, Front. Microbiol. 10 (2019) 1, https://doi.org/10.3389/fmicb.2019.00911.

[12] Arunagiri Santhosh Kumar, Lakshminarayanan Sivakumar, Suriyaprakash Rajadesingu, Sambath Sathish, Tabarak Malik, Punniyakotti Parthipan, Sustainable corrosion inhibition approaches for the mitigation of microbiologically influenced corrosion -a systematic review, Front. Mater. 12 (2025), https://doi.org/10.3389/fmats.2025.1545245.

[13] G. Zlatić, I. Martinović, Z. Pilić, I. Kodranov, J. Ciganović, V. Sokol, The effect of Artemisia annua L. extract on microbiologically influenced corrosion of A36 steel caused by Pseudomonas aeruginosa, Bioelectrochemistry 152 (2023) 108447, https://doi.org/10.1016/j.bioelechem.2023.108447.

[14] G. Zlatić, I. Martinović, Z. Pilić, J. Kovač, S. Čelan, Electrochemical behavior of Artemisia annua extract on 5083 aluminium alloy in marine environment, J. Electroanal. Chem. 975 (2024) 118727, https://doi.org/10.1016/j.jelechem.2024.118727.

[15] Gloria Zlatić Jelić, Ivana Martinović, Zora Pilić, Inhibition of microbiologically influenced corrosion of 304 stainless steel by Artemisia annua L. in simulated seawater, Alloys 4 (4) (2025) 20, https://doi.org/10.3390/alloys4040020.

[16] G. Zlatić, I. Martinović, Z. Pilić, A. Paut, I. Mitar, A. Prkić, D. Čulum, Green inhibition of corrosion of aluminium alloy 5083 by Artemisia annua L. extract in artificial seawater, Molecules 28 (2023) 2898.

[17] H.C. Qian, W.W. Chang, W.L. Liu, T.Y. Cui, Z. Li, D.W. Guo, C.T. Kwok, L.M. Tam, D.W. Zhang, Investigation of microbiologically influenced corrosion inhibition of 304 stainless steel by D-cysteine in the presence of Pseudomonas aeruginosa, Bioelectrochemistry 143 (2022) 107953, https://doi.org/10.1016/j.bioelechem.2021.107953.

[18] Gloria Zlatić, The Influence of Sweet Wormwood Extract (Artemisia annua L.) on the Formation of an Oxide Film of Alloys in Artificial Seawater in the Presence of the Bacterium Pseudomonas aeruginosa, PhD Dissertation, University of Split, 2024, https://urn.nsk.hr/urn:nbn:hr:167:758587.

[19] J.F. Moulder, W.F. Stickle, P.E. Sobol, K.D. Bomben, Handbook of X-Ray Photoelectron Spectroscopy, Physical Electronics Inc., Eden Prairie, Minnesota, USA, 1995.

[20] Wan Mohamad Ikhmal Wan Mohamad Kamaruzzaman, Muhamad Syaizwadi Shaifudin, Nursabrina Amirah Mohd Nasir, Malia Athirah Badruddin, Nusaibah Yusof, Azila Adnan, Norazlina Abdul Aziz, Wan Mohd Norsani Wan Nik, Jiyaul Haque, Manilal Murmu, Priyabrata Banerjee, Mohd Sabri Mohd Ghazali, Experimental, DFT and molecular dynamic simulation of Andrographis paniculata as corrosion inhibitor for mild steel in artificial seawater, Mater. Chem. Phys. 312 (2024) 128642, https://doi.org/10.1016/j.matchemphys.2023.128642.

[21] L. Nguyen, T. Hashimoto, D.N. Zakharov, E.A. Stach, A.P. Rooney, Be Berkels, G. E. Thompson, S.J. Haigh, T.L. Burnett, Atomic-scale insights into the oxidation of aluminum, ACS Appl. Mater. Interfaces 10 (2018) 3, https://doi.org/10.1021/acsami.7b17224.

[22] M. Chellouli, D. Chebabe, A. Dermaj, H. Erramli, N. Bettach, N. Hajjaji, M. P. Casaletto, C. Cirrincione, A. Privitera, A. Srhiri, Corrosion inhibition of iron in acidic solution by a green formulation derived from Nigella sativa L, Electrochim. Acta 204 (2016) 50–58, https://doi.org/10.1016/j.electacta.2016.04.015.

[23] R. Zhang, D. Sur, K. Li, J. Witt, R. Black, A. Whittingham, J.R. Scully, J. Hattrick-Simpers, Bayesian assessment of commonly used equivalent circuit models for corrosion analysis in electrochemical impedance spectroscopy, npj Mater. Degrad. 8 (2024) 120, https://doi.org/10.1038/s41529-024-00537-8.

[24] Y. Lekbach, Z. Li, D. Xu, S. El Abed, Y. Dong, D. Liu, T. Gud, S.I. Koraichi, K. Yangc, F. Wang, Salvia officinalis extract mitigates the microbiologically influenced corrosion of 304L stainless steel by Pseudomonas aeruginosa biofilm, Bioelectrochemistry 128 (2019) 193, https://doi.org/10.1016/j.bioelechem.2019.04.006.

[25] Carlos M. Menendez, Application of optical profilometric techniques to corrosion monitoring.". Proceedings of the CORROSION 2013, CORROSION, Orlando, FL, 2013, pp. 1–16, https://doi.org/10.5006/C2013-02506. AMPP.

[26] Hongchang Qian, Shangyu Liu, Pei Wang, Ye Huang, Yuntian Lou, Luyao Huang, Chengying Jiang, Dawei Zhang, Investigation of microbiologically influenced corrosion of 304 stainless steel by aerobic thermoacidophilic archaeon Metallosphaera cuprina, Bioelectrochemistry 136 (2020) 107635, https://doi.org/10.1016/j.bioelechem.2020.107635.

[27] H. Cui, W. Ren, P. Lin, Y. Liu, Structure control synthesis of iron oxide polymorph nanoparticles through an epoxide precipitation route, J. Exp. Nanosci. 8 (2013) 869, https://doi.org/10.1080/17458080.2011.61654.

[28] M.M. Ayad, N.L. Torad, A. Abu El-Nasr, W.A. Amer, Study on catalytic efficiency of platinum and silver nanoparticles confined in nanosized channels of a 3-D mesostructured silica, J. Porous Mater. 28 (2021) 65, https://doi.org/10.1007/s10934-020-00960-7.

[29] I.B. Beech, J. Sunner, Biocorrosion: towards understanding interactions between biofilms and metals, Curr. Opin. Biotechnol. 15 (3) (2004) 181–186, https://doi.org/10.1016/s0958-1669(04)00063-12.

[30] T. Gu, D. Wang, Y. Lekbach, D. Xu, Extracellular electron transfer in microbial biocorrosion, Curr. Opin. Electrochem. 29 (2021) 100763, https://doi.org/10.1016/j.coelec.2021.100763.

[31] H.C. Flemming, The perfect slime, Colloids Surf., B 86 (2011) 251–259, https://doi.org/10.1016/j.colsurfb.2011.04.025.

[32] Michael B. Hay, Satish C.B. Myneni, Structural environments of carboxyl groups in natural organic molecules from terrestrial systems. Part 1: infrared spectroscopy, Geochem. Cosmochim. Acta 71 (2007) 3518–3532, https://doi.org/10.1016/j.gca.2007.03.038.

[33] S. Pasieczna-Patkowska, M. Cichy, J. Flieger, Application of fourier transform infrared (FTIR) spectroscopy in characterization of green synthesized nanoparticles, Molecules 30 (3) (2025) 684, https://doi.org/10.3390/molecules30030684.

[34] T. Carbonara, R. Pascalea, M-a Argentieria, P. Papadiab, F.-P. Fanizzib, L. Villanovac, P. Avatoa, Phytochemical analysis of a herbal tea from Artemisia

annua L, JPBA Open 62 (2012) 79–86, https://doi.org/10.1016/j.jpba.2012.01.015.
[35] Hoda Hamidi, Fazel Shojaei, Mahdi Pourfath, Mehdi Vaez-Zadeh, Adsorption behavior of some green corrosion inhibitors on Fe (110) surface: the critical role of d-π interactions in binding strength, Appl. Surf. Sci. 655 (2024) 159425, https://doi.org/10.1016/j.apsusc.2024.159425.
[36] Menglin Guo, Ran Zhang, Chenge Zhang, Fuqiang Liang, Jiayi Shi, Impact of covalent interactions between caffeic acid and rice bran albumin on protein structure and function, Food Chem. 506 (2026) 148173, https://doi.org/10.1016/j.foodchem.2026.148173.
[37] V. Sindhu, S. Sharma, A.K. Mishra, S.S. Singh, Caffeic acid from desikacharya sp. TPB-4: a sustainable source with antimicrobial potential against Aeromonas caviae, Arch. Microbiol. 208 (2026) 32, https://doi.org/10.1007/s00203-025-04553-3.